Ultrafast diffraction and structural dynamics: The nature of complex molecules far from equilibrium

Chong-Yu Ruan, Vladimir A. Lobastov, Ramesh Srinivasan, Boyd M. Goodson, Hyotcherl Ihee, and Ahmed H. Zewail*

Laboratory for Molecular Sciences, Arthur Amos Noyes Laboratory of Chemical Physics, California Institute of Technology, Pasadena, CA 91125

Contributed by Ahmed H. Zewail, April 19, 2001

Studies of molecular structures at or near their equilibrium configurations have long provided information on their geometry in terms of bond distances and angles. Far-from-equilibrium structures are relatively unknown—especially for complex systems—and generally, neither their dynamics nor their average geometries can be extrapolated from equilibrium values. For such nonequilibrium structures, vibrational amplitudes and bond distances play a central role in phenomena such as energy redistribution and chemical reactivity. Ultrafast electron diffraction, which was developed to study transient molecular structures, provides a direct method for probing the nature of complex molecules far from equilibrium. Here we present our ultrafast electron diffraction observations of transient structures for two cyclic hydrocarbons. At high internal energies of ≈4 eV, these molecules display markedly different behavior. For 1,3,5-cycloheptatriene, excitation results in the formation of hot ground-state structures with bond distances similar to those of the initial structure, but with nearly three times the average vibrational amplitude. Energy is redistributed within 5 ps, but with a negative temperature characterizing the nonequilibrium population. In contrast, the ring-opening reaction of 1,3-cyclohexadiene is shown to result in hot structures with a C—C bond distance of over 1.7 Å, which is 0.2 Å away from any expected equilibrium value. Even up to 400 ps, energy remains trapped in large-amplitude motions comprised of torsion and asymmetric stretching. These studies promise a new direction for studying structural dynamics in nonequilibrium complex systems.

The premise of ultrafast electron diffraction (UED) is similar to ultrafast spectroscopies (for recent work from this laboratory, see refs. 1–5): a femtosecond laser pulse excites the molecules, and a second pulse, in this case a picosecond burst of electrons, probes the resulting structural evolution with the zero-of-time precisely determined *in situ*. With UED, the changing nuclear coordinates are directly recorded in time-dependent diffraction patterns. By timing the electron pulses to arrive before the light pulses, ground-state diffraction images are obtained at negative times. Time-resolved diffraction snapshots of the transient molecular structures are then recorded at positive times by varying the time delay between light and electron pulses. In the present work, we prepare vibrationally hot structures by radiationless transfer after the initial photon absorption and/or as a result of a chemical reaction. Scheme 1 depicts the two reactions that are the subject of this contribution.

Concepts of Equilibrium vs. Nonequilibrium Structures. Differences between diffraction patterns of structures at equilibrium and those far from equilibrium can be understood by first considering the case of a single bond (Fig. 1). The diffraction of structures far from equilibrium manifests itself as (*i*) increased damping of the oscillating molecular scattering signal; and (*ii*) apparent shifts in internuclear distance(s). As seen in Fig. 1*a*, simple thermal heating of the molecule results in nearly the same average internuclear distance (r), but its vibrational amplitude (l) increases with temperature. This elevated l value can be readily observed as enhanced damping of the modified molecular scattering signal [$sM(s)$]; the relevant dependence is given by (6):

$$sM(s) \propto \frac{\sin(sr)}{r} \cdot \exp(-\tfrac{1}{2}l^2s^2), \qquad [1]$$

where s is the momentum transfer parameter. This damping is mirrored as broadened peaks in the radial distribution curve [$f(r)$] because of its Fourier (sine) transform relation to $sM(s)$. The damping reflects thermal averaging over the vibrational states in a Boltzmann distribution, given in the harmonic limit (l_h) as (6)

$$\langle l_h^2 \rangle = \frac{h}{8\pi^2\mu\nu} \coth\left(\frac{h\nu}{2kT}\right), \qquad [2]$$

where μ is the reduced mass, ν is the vibrational frequency, k is the Boltzmann constant, and T is the vibrational temperature. In the limit of high energy, $\langle l_h^2 \rangle$ scales linearly with the vibrational temperature.

In contrast to this thermal (Boltzmann) preparation where the structures are near equilibrium, structures far from equilibrium would result if the system were prepared with inverted (non-Boltzmann) distributions (7). Fig. 1*b* shows our calculations for the case where wave packets are produced with Gaussian energy distributions at different mean energies, which in turn give rise to the corresponding probability densities in the long-time limit. Significantly inverted populations would lead to a clear bifurcation of the internuclear density, inducing splitting and shifting of peaks in the $f(r)$ curve—which gives the relative populations of internuclear distances. However, in the case where these non-Boltzmann populations occur at relatively low energies in the potential well, the density bifurcation becomes narrower, and the $f(r)$ curve may not display shifted peaks, but would exhibit increased damping, thus mimicking Boltzmann distributions albeit with exceptionally high l values. These concepts of enhanced damping and shifted bond distances, shown here for a molecule with a single bond far from equilibrium, are directly relevant to complex molecular structures where energy redistribution may or may not be complete, and where certain bonds determine the reaction coordinate.

Experimental Methodology. UED data were obtained with our third-generation apparatus (2), which will be described in greater detail in a separate publication from this laboratory. Briefly, the amplified output from a Ti/Sapphire laser system (≈350 μJ, ≈120 fs, 267 nm, 1 kHz repetition rate) was split into two beams, with the stronger beam being directed into the scattering chamber to initiate the reaction. The weaker beam was directed into a delay line and then focused onto a back-illuminated photocathode to generate electron pulses via the photoelectric effect (30 kV, de Broglie wavelength: λ = 0.067 Å, ≈25,000 electrons per pulse at ≈4 ps). The molecular sample was introduced into the chamber via a jet expansion source. After interacting with the molecular beam, the diffracted electrons were detected with a low-noise charge-coupled device camera [active s range: ≈1.5–18.5 Å; $s = (4\pi/\lambda)\cdot\sin(\theta/2)$, where θ is the scattering angle]. Samples of 1,3,5-cycloheptatriene (CHT) (Fluka, 95%) and 1,3-cyclohexadiene (CHD) (Aldrich,

Abbreviations: UED, ultrafast electron diffraction; CHT, 1,3,5-cycloheptatriene; CHD, 1,3-cyclohexadiene; HT, 1,3,5-hexatriene; *cZc*, *di-s-cis-Z*-hexatriene; *cZt*, *mono-s-cis-Z*-hexatriene; *tZt*, *di-s-trans-Z*-hexatriene.

*To whom reprint requests should be addressed. E-mail: zewail@caltech.edu.

The publication costs of this article were defrayed in part by page charge payment. This article must therefore be hereby marked "*advertisement*" in accordance with 18 U.S.C. §1734 solely to indicate this fact.

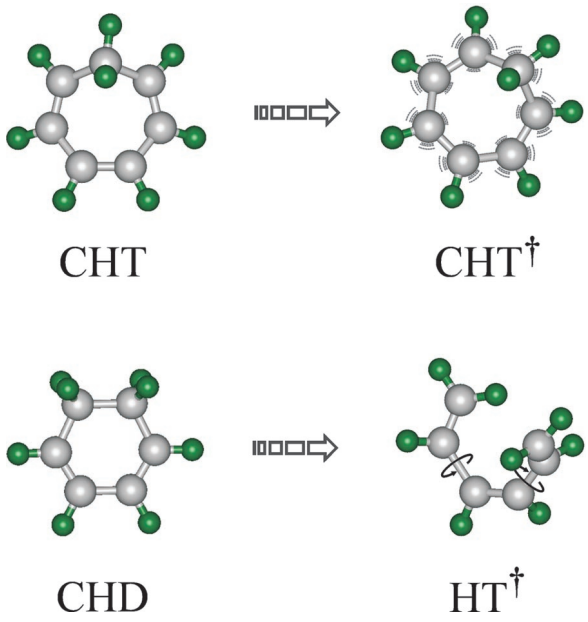

Scheme 1.

97%) were degassed with several freeze-pump-thaw cycles, and high-purity xenon (Spectra Gases, 99.999%) was used as an atomic reference gas (8). The nozzle temperature for the diffraction experiments was maintained at 130 and 120°C for CHT and CHD, respectively. To establish the point of reference for temporal studies, the zero of time was determined via photoionization-induced lensing (9) of the undiffracted electron beam by using CF_3I gas (Aldrich, 99%).

Data Processing and Analysis. Two-dimensional diffraction images acquired at varying time delays were radially averaged to generate one-dimensional total intensity curves, from which experimental $sM(s)$ curves were calculated (6). To highlight the structural changes occurring over the course of the reaction, time-dependent difference curves were generated by subtracting a reference diffraction signal (obtained at negative time) from the signals at positive times. As they contain equal but opposite contributions from the parent and product structures, difference curves permit the relative parent and product fractions to be determined at each point in time (10). Finally, to isolate the contribution from the product structures, product-only curves were generated by adding the appropriately scaled parent diffraction signal to the difference curves, thereby canceling out the parent component in each curve (11).

By using *ab initio* or previously available experimental structural parameters, geometrically consistent molecular models were constructed, from which theoretical $sM(s)$ curves were derived. A Monte Carlo sampling procedure was then applied to seek out structures corresponding to χ^2 minima in configuration space, followed by least-squares refinement of the structures. Vibrationally excited structures were modeled by correcting for the increased l values; l values for thermally equilibrated structures were either estimated with the ASYM40 program (12) or extrapolated to high temperatures by using empirical equations (13, 14). Extrapolated l values were also used to relate r_e (the equilibrium internuclear distance at the potential minimum), to r_a (the internuclear distance measured by electron diffraction), by using the equation:

$$r_a \approx r_e + \tfrac{3}{2}\, a \cdot l^2 + dr - \frac{l^2}{r_e}, \qquad [3]$$

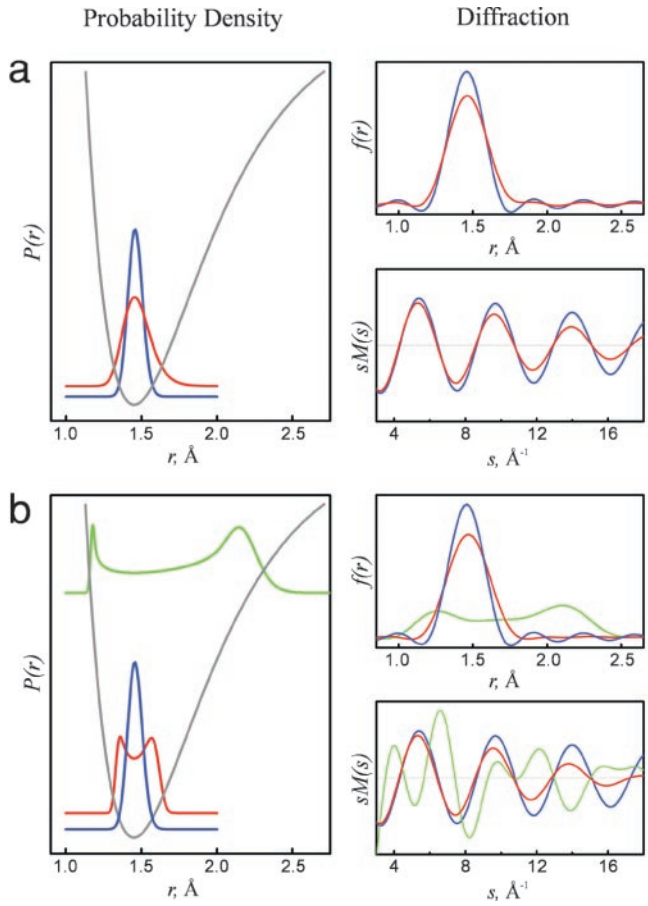

Fig. 1. Calculated diffraction curves for a single bond in two regimes: Boltzmann distribution and non-Boltzmann distribution. Shown on the *Left* are probability densities of the single bond distance, and on the *Right* are the resulting molecular scattering signals [$sM(s)$] and radial distribution curves [$f(r)$]. (*a*) Thermal (Boltzmann) vibrational population at low temperature (blue) and at a much higher temperature (red). Increased temperature results in broadening of the $f(r)$ curve and damping of the $sM(s)$ curve. (*b*) Inverted (non-Boltzmann) vibrational populations modeled with Gaussian distributions. Low-lying inverted populations (red) will cause broadening of the $f(r)$ curve and damping of the $sM(s)$ curve similar to the Boltzmann case above. Higher-lying populations (green) can lead to outright bifurcation of the internuclear density and significant changes in the frequency components of the $sM(s)$ scattering signal.

where a is the anharmonicity constant for the bond, and dr is a small correction for centrifugal distortion (6).

Results and Discussion

Ground State. Fig. 2 shows typical ground-state diffraction images for CHT and CHD and the corresponding structures. Differences between the ring patterns of the two species are evident even in the two-dimensional images, demonstrating the high sensitivity and resolution of our third-generation UED apparatus (2). The major peaks in the $f(r)$ curves reflect relative populations of various C—C distances (in CHT, for example, covalent distances occur at ≈1.4 Å, second-nearest neighbor at ≈2.5 Å, and third-nearest neighbor at ≈3.0 Å). The $f(r)$ curve for CHD clearly shows much lower density of third-nearest neighbor C··C distances compared with CHT. Both curves are in good agreement with previous results obtained with conventional electron diffraction (15, 16) and with our own *ab initio* predictions.

Structural Dynamics of CHT. On excitation, CHT undergoes an ultrafast hydrogen shift (17–20), but with subsequent reformation of CHT at high internal energy. Except for their relative intensities,

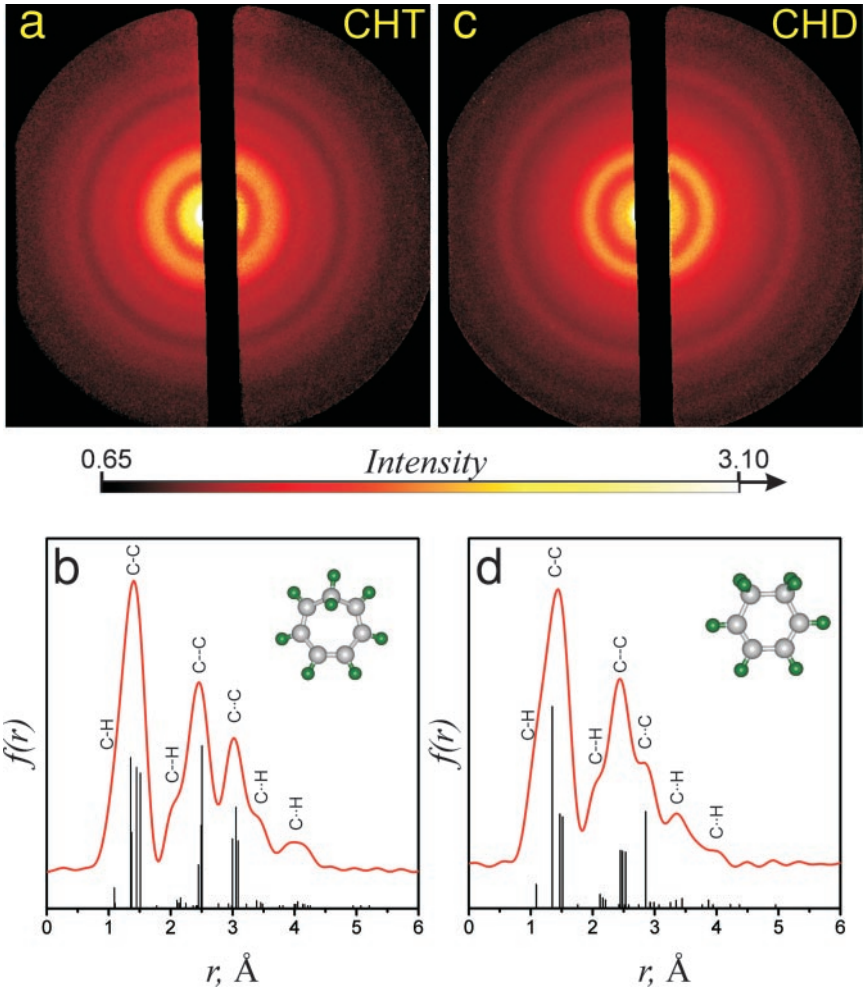

Fig. 2. Observed ground-state diffraction images and corresponding $f(r)$ curves for CHT (*a*, *b*) and CHD (*c*, *d*). The vertical lines in *b* and *d* approximate the relative contributions from various internuclear pairs; the height of each line scales with $(Z_iZ_j)^2/r_{ij}$ multiplied by the degeneracy, where Z is the nuclear charge and r_{ij} is the internuclear distance. The major bond distances (covalent C—C, second nearest-neighbor C- -C, and third nearest-neighbor C··C) are shown above the corresponding $f(r)$ peaks.

all of the product-only $sM(t; s)$ curves were nearly indistinguishable. Fig. 3 shows the experimental $sM(s)$ curve averaged from 75 to 400 ps, along with theoretical curves with the same internuclear distances as those of the initial structure (15), but with varying l values. It is evident that the experimental curve is significantly more damped than the theoretical curve (for the initial structure) at 403 K, clearly establishing the "hotness" of product CHT. If the initially deposited energy (107 kcal/mol) were equipartitioned among the CHT modes (21) with a Boltzmann distribution within their vibrational levels (see Fig. 1*a*), the molecule would have an internal temperature of ≈2,200 K (per mode). However, the poor fit of this thermalized model with our experimental data precludes Boltzmann vibrational distributions.

Indeed, excellent agreement is obtained between experiment and theory with l values whose mean is nearly three times that at equilibrium, indicating a non-Boltzmann distribution in the vibrational levels. This dramatic increase in the vibrational amplitudes compared with those resulting from a Boltzmann assumption suggests that the hot (product) structure can be characterized by a negative temperature, wherein the upper vibrational levels have higher population than the lower levels. Note the similarity in frequency components between the theoretical $sM(s)$ curve for the equilibrium structure (at 403 K) and the experimental curve, indicating that internuclear distances (in the product) are nearly identical to those at equilibrium, in turn implying nearly complete energy redistribution.

Fig. 4 shows the structural evolution of the CHT product, obtained by fitting the growing intensity of the $sM(t; s)$ curves with increasing time delay. Previous ultrafast spectroscopic studies (see, for example, ref. 18) have suggested that conical intersections are responsible for the ultrafast formation of product in tens to hundreds of femtoseconds. However, our structural dynamics studies indicate that the hot structure must be formed on a time scale of 16 ± 3 ps. This longer time scale implies that the product is formed via an avoided crossing or by longer-lived trajectories on the excited surface that involve intramolecular vibrational-energy redistribution; see below. This is not surprising, as other studies on the femtosecond time scale (see, for example, refs. 22–24) have shown the existence of a distribution of femtosecond and picosecond trajectories as molecules traverse a complex energy landscape. If all trajectories were on the femtosecond time scale and we were merely observing picosecond energy redistribution, our $sM(s)$ curves would have revealed structural changes as a function of time. On the other hand, if the structure were that of the excited state, the vibrational temperture would be much lower than that indicated above. It should be noted that UED probes the changes of *all* nuclear coordinates, and therefore the dynamics reported here are directly relevant to global structural changes in the molecule. In contrast, spectroscopic studies reported for the gas phase (ref. 18; femtoseconds) and condensed phase (ref. 17; 26 ± 10 ps) monitor state populations. The roles of the solvent and intramolecular relaxation must be disentangled before direct comparisons can be made with our results of the isolated reaction dynamics.

Structural Dynamics of CHD. In reactive systems, where bonds are broken and formed, the partitioning of energy may result in its localization in certain bonds associated with the reaction coordinate. Indeed, we observed incomplete energy partitioning even up

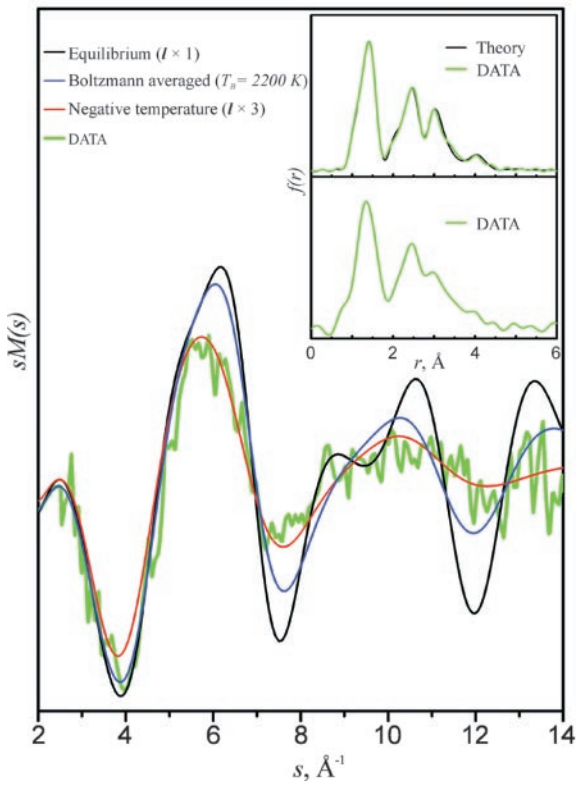

Fig. 3. UED of CHT: product-only *sM*(*s*) curves. The (green) experimental curve averaged from 75 to 400 ps is shown, along with corresponding theoretical curves for the equilibrium structure at 403 K (black), the Boltzmann averaged structure at ≈2,200 K (blue), and a non-Boltzmann structure with a mean *I* value nearly three times that at 403 K (red). For details of structural analysis, see text. The *Inset* shows the *f*(*r*) curves for the initial structure at 403 K (*Top*) and the hot CHT structure at a negative temperature (*Bottom*; see text). Note the significant broadening of the *f*(*r*) peaks in the hot structure.

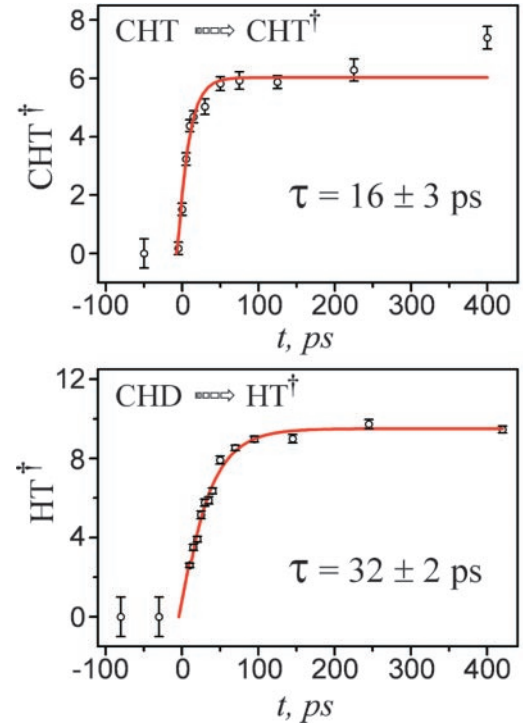

Fig. 4. Time evolution of the hot CHT and hot HT fractions (in percent) from the reaction of CHT and CHD, respectively.

to 400 ps in hot 1,3,5-hexatriene (HT), formed by the ultrafast ring opening of CHD (25–28). Fig. 5 shows the evolution of radial distribution curves for the ring-opening reaction of CHD. The product-only HT diffraction curves were significantly damped at all time points [manifested as peak broadening in the *f*(*t*; *r*) curves], indicating the vibrationally hot nature of the product structure; however, unlike CHT, new peaks appear in *f*(*r*). Shown below the experimental data in Fig. 5 are theoretical *f*(*r*) curves for three hot conformers of HT (labeled *cZc*, *cZt*, and *tZt* with respect to the conformation of torsion angles about the C—C single bonds; see Fig. 6). Close inspection of the experimental *f*(*t*; *r*) curves reveals greater similarity to the theoretical *cZc* curve than to that of the lower-energy *tZt* conformer. Furthermore, an anomalous peak at ≈1.7 Å can be seen as a shoulder in all of the experimental *f*(*t*; *r*) curves; the presence of this peak, which is about 0.2 Å away from expected equilibrium C—C distances, was found to be reproducible in repeated diffraction experiments.

Least-squares refinement of the structural parameters yielded a HT molecular structure at each time slice; to locate the global minimum, Monte Carlo techniques were first applied for searching the configuration space, and finally the structure at each time represents the average over the local minima closest to the global minimum. These HT structures showed no *tZt* character, but consistently manifested a configuration intermediate between *cZc* and *cZt*, far removed from a thermally equilibrated conformer distribution of ≈41% *tZt*, ≈45% *cZt*, and ≈14% *cZc* at 2,100 K (estimated from *ab initio* calculations of the conformer energies). Moreover, the ≈1.7 Å peak observed in the *f*(*t*; *r*) curves was assigned to one C—C single bond in HT—a highly nonequilibrium value for a C—C internuclear separation. The remarkable departure from the predicted equilibrium conformation, together with the unusual C—C bond length, confirms the far-from-equilibrium nature of the HT structure.

The hot HT structure is formed with a time constant of 32 ± 2 ps (Fig. 4) and remains virtually unchanged over the course of the experiment (400 ps) as shown in Fig. 5. Time-averaged values for selected structural parameters are summarized in Table 1, along with corresponding *ab initio* values for the three HT conformers. The persistence of this far-from-equilibrium structure even up to 400 ps indicates that unlike CHT, energy partitioning within HT is slow with respect to both the rate of product formation and the time scale of the UED experiment. The existence of a *cZc*-like conformation clearly indicates an inverted population on the potential energy surface (projected along the coordinate of torsional motion), with significant density at the classical turning points; this coherent nuclear motion is shown schematically in Fig. 6. Moreover, the ≈1.7 Å distance assigned to a C—C bond would require ≈15 kcal/mol of the available ≈90 kcal/mol to be deposited in that C—C bond (assuming a simple Morse oscillator model), providing further evidence for an inequitable partitioning of energy. Note that if energy partitioning were indeed complete, then each of the 36 modes in HT would have ≈2.5 kcal/mol.

Coexistence of the two structural features—an inverted torsional conformation and a stretched C—C bond—over time strongly suggests a long-lived, low-frequency hybrid motion comprised of both torsion and asymmetric stretching of the carbon skeleton. Conceptually, one may picture that as the molecule oscillates between the turning points of the potential well (Fig. 6), the stretched C—C distance is shifted continuously from one C—C single bond to another, and at the turning points, the torsional energy is partially stored in the C—C bond stretch. That this far-from-equilibrium structure lasts for over 400 ps suggests a bottleneck in energy transfer from the inferred hybrid motion to

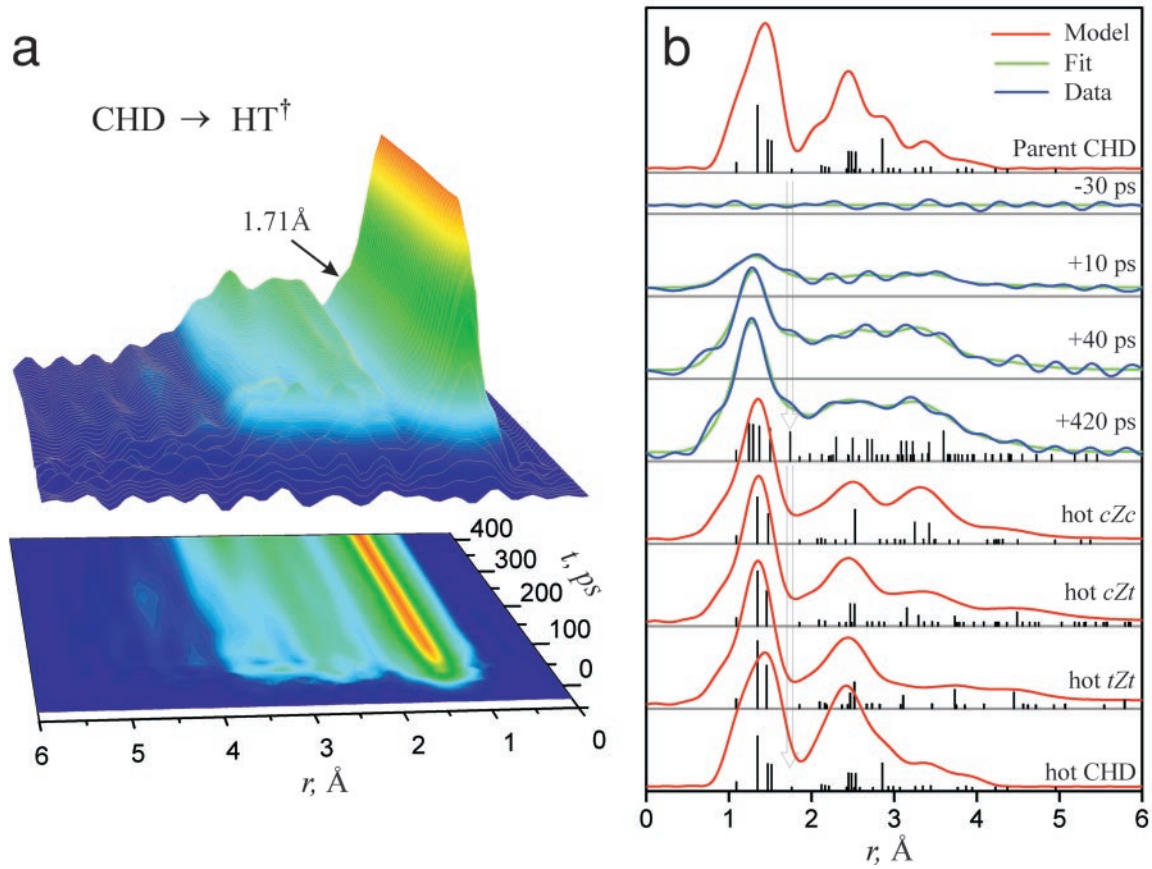

Fig. 5. UED of CHD: time-resolved formation of hot HT structures after the ring opening of CHD. (*a*) Fourier-filtered *f*(*t; r*) curves showing product evolution; note the shoulder at ≈1.7 Å. (*b*) *Top*: *ab initio* f(*r*) curve (red) for the CHD parent structure at 403 K. *Middle*: comparison of selected experimental product-only *f*(*t*; *r*) curves (blue) with corresponding structural fits (green). *Bottom*: *ab initio* f(*r*) curves (red) for the three HT conformers (extrapolated to 2,100 K) and for hot CHD (extrapolated to 2,400 K) shown for comparison. These temperatures were estimated from frequencies reported in refs. 36 and 37, respectively. The vertical arrows indicate the peak at ≈1.7 Å, which is present in all experimental curves, but which is absent in the *ab initio* f(*r*) curves of the three HT conformers.

other (higher frequency) modes, after the initial energy deposition. This energy localization could result from a mismatch in the frequencies of the coherent modes compared with all other modes (at these high internal energies). It is interesting to note here that torsional modes of this type have been isolated in dynamical calculations of polypeptides (29).

Ultrafast spectroscopic studies of the CHD ring opening reaction have suggested contrasting time scales for the formation of the HT product—tens to hundreds of femtoseconds (26–28) and 6 ± 1 ps (25)—with the presence of conical intersections invoked to rationalize the ultrafast time scales. The initial preparation of CHD is to the S_2 excited state; the S_2/S_1 conical intersection is along the readily accessible symmetric path (see below) and gives rise to femtosecond dynamics. Accordingly, the crossing/avoided-crossing to the ground state (S_0) determines the longer picosecond time scale of the dynamics. It is interesting to note that, although we found virtually no contribution from hot CHD in the HT product diffraction patterns (despite our sensitivity to hot "parent" structures in CHT), static condensed-phase experiments have reported a 60/40 branching ratio for the CHD reformation/ring-opening pathways (30). This near absence of hot parent structures, along with the long time observed by UED for ring opening, signifies the crucial role played by the solvent (in contrast to the isolated molecule) in redirecting the fate of the reaction. For instance, the increased steric hindrance to ring opening in the solvent may favor the reformation of CHD over ring opening. Moreover, the solvent can induce slight pertur-

Table 1. Selected refined structural parameters for the far-from-equilibrium HT structure

Structural parameter	Mean value*	σ_{mean}†	σ_{fit}‡	cZc§	cZt§	tZt§
r(C1═C2)	1.29 Å	0.06 Å	0.04 Å	1.338 Å	1.342 Å	1.342 Å
r(C2—C3)	1.40 Å	0.10 Å	0.02 Å	1.471 Å	1.453 Å	1.452 Å
r(C3═C4)	1.41 Å	0.08 Å	0.04 Å	1.350 Å	1.353 Å	1.355 Å
r(C4—C5)	1.71 Å	0.05 Å	0.02 Å	1.471 Å	1.465 Å	1.452 Å
r(C5═C6)	1.32 Å	0.04 Å	0.03 Å	1.338 Å	1.341 Å	1.342 Å
ϕ_1(C1C2—C3C4)	84°	41°	11°	35.5°	−174.7°	180°
ϕ_2(C3C4—C5C6)	15°	22°	11°	35.5°	37.7°	180°

*Structural parameters obtained from averaging over all time points.
†Standard deviation (spread) of the mean value.
‡Standard deviation (error) of the least-squares fit.
§Structural parameters for the HT conformers, calculated by using *ab initio* methods (38) (B3LYP/6-311G** basis set), shown for comparison.

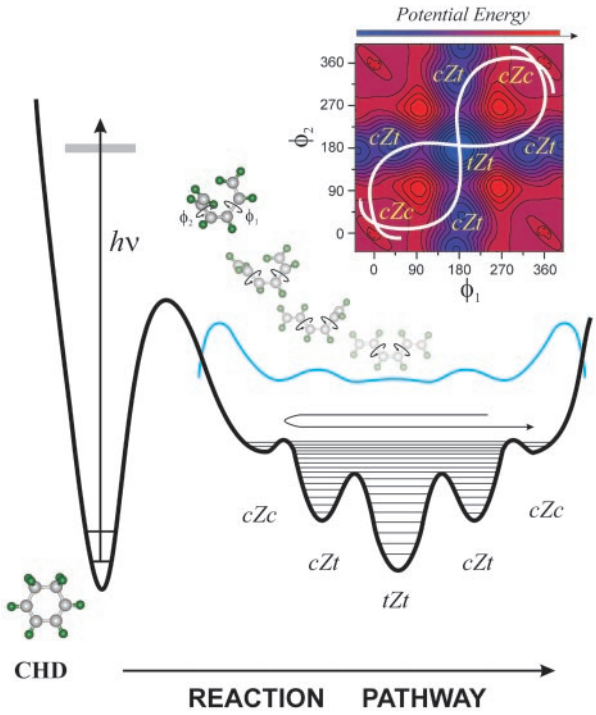

Fig. 6. Potential energy landscape relevant to the formation of HT. A probability density curve (blue) on the schematic HT ground-state surface depicts the high-energy nature of the product structure. The higher density near the classical turning points reflects significant population in *cZc*-type conformations; the refined molecular structure shown at one of these points represents the average far-from-equilibrium structure over 400 ps. The ''faded'' structures denote the lower-energy *cZc*, *cZt*, and *tZt* conformations. The *Inset* shows the corresponding *ab initio* two-dimensional potential energy surface governing HT torsion angles (ϕ_1 and ϕ_2) about the C—C single bonds. The white curves illustrate possible trajectories leading to a time-averaged structure with considerable *cZc* and *cZt* character, but virtually no contribution from *tZt*.

bations in the relative positions of the potential energy surfaces, which can dramatically alter the time scales (23) for reaction in the condensed phase.

The above diffraction experiments for CHT and CHD also reflect the nature of the nascent structures born at the point of descent to the ground state surface (the "transition state"). Both reactions have been the subject of recent *ab initio* calculations (19, 31). These calculations have suggested the existence of two regions on the excited-state energy surface, determined by the C–C stretch motion and the ring-bending motion (a precuror to torsions). Also, the molecular structure at the conical intersection is highly distorted. If the conical intersection is reached directly in the initial motion, then femtosecond dynamics result; otherwise, intramolecular vibrational-energy redistribution is needed to redirect the trajectories. For example, at the point of descent from the excited state, CHT must adopt a near-planar geometry (as opposed to the minimum-energy boat-shaped geometry at equilibrium) for the [1,7]-sigmatropic hydrogen shift reaction to occur. Thus, efficient energy redistribution is essential in this transformation to the final geometry via a planar "transition state." On the other hand, ring opening in CHD lands the structure in a highly asymmetric geometry on the ground state and, except for the subsequent hybrid (torsional and bond stretching) motion, the nature of the system is similar to that of the final product. In other words, the nonequilibrium features of the HT structure may reflect memory of an asymmetric geometry at the instant of ring opening, suggesting that ring opening of CHD follows a symmetry-breaking pathway that violates the C_2 symmetry of the parent structure (31). However, although the *ab initio* calculations (31) were performed for the minimum energy path, we are concerned here with nuclear dynamics of far-from-equilibrium structures. Thus, our diffraction results illustrate the crucial role played by structural changes in directing the subsequent dynamics in nuclear subspace (on the ground potential surface) of the reaction.

Conclusions

We have demonstrated the ability of ultrafast diffraction to observe the time evolution of molecular structures in nonequilibrium configurations. Although nonthermal effects have been previously reported (see, for example, refs. 5, 7, 32–35), to our knowledge this is the first time that such far-from-equilibrium structures, in terms of both vibrational amplitudes and bond distances, have been directly observed in isolated complex molecules. The concept of negative temperature was invoked to describe the observed populations at high internal energies. The structural dynamics of the two hydrocarbons studied here underscore the importance of the following issues: (*i*) the critical influence of structural changes on energy redistribution and on persistence of certain bond motions; (*ii*) the nature of the nascent structure(s) born en route to the final product and the associated coherent dynamics; and (*iii*) the direct relevance of structural changes associated with bond breaking and making in understanding the disparities of measured time scales for state population dynamics in the condensed phase. With the added dimensions of time and complexity, ultrafast electron diffraction is now poised to explore the structural and energetic features underlying transient conformational changes in chemical and biological systems.

This work was supported by the National Science Foundation and the Air Force Office of Scientific Research.

1. Williamson, J. C., Cao, J., Ihee, H., Frey, H. & Zewail, A. H. (1997) *Nature (London)* **386,** 159–162.
2. Ihee, H., Lobastov, V. A., Gomez, U., Goodson, B. M., Srinivasan, R., Ruan, C.-Y. & Zewail, A. H. (2001) *Science* **291,** 458–462.
3. Helliwell, J. (2001) *Phys. World* **14,** 25.
4. Ihee, H., Cao, J. & Zewail, A. H. (2001) *Angew. Chem. Int. Ed. Engl.* **40,** 1532–1536.
5. Zewail, A. H. (2000) *Angew. Chem. Int. Ed. Engl.* **39,** 2587–2631.
6. Hargittai, I. & Hargittai, M. (1988) *Stereochemical Applications of Gas-Phase Electron Diffraction* (VCH, New York).
7. Ischenko, A. A., Schäfer, L., Luo, J. Y. & Ewbank, J. D. (1994) *J. Phys. Chem.* **98,** 8673–8678.
8. Lobastov, V. A., Ewbank, J. D., Schäfer, L. & Ischenko, A. A. (1998) *Rev. Sci. Instrum.* **69,** 2633–2643.
9. Dantus, M., Kim, S. B., Williamson, J. C. & Zewail, A. H. (1994) *J. Phys. Chem.* **98,** 2782–2796.
10. Ihee, H., Cao, J. & Zewail, A. H. (1997) *Chem. Phys. Lett.* **281,** 10–19.
11. Cao, J., Ihee, H. & Zewail, A. H. (1998) *Chem. Phys. Lett.* **290,** 1–8.
12. Hedberg, L. & Mills, I. M. (1993) *J. Mol. Spectrosc.* **160,** 117–142.
13. Mastryukov, V. S. & Cyvin, S. J. (1975) *J. Mol. Struct.* **29,** 15–25.
14. Mastryukov, V. S., Osina, E. L., Vilkov, L. V. & Cyvin, S. (1976) *J. Struct. Chem.* **17,** 64–68.
15. Traetteberg, M. (1964) *Act. Chem. Scand.* **86,** 4265–4270.
16. Oberhammer, H. & Bauer, S. H. (1969) *J. Am. Chem. Soc.* **91,** 10–16.
17. Reid, P. J., Shreve, A. P. & Mathies, R. A. (1993) *J. Phys. Chem.* **97,** 12691–12699.
18. Trushin, S. A., Diemer, S., Fuss, W., Kompa, K. L. & Schmid, W. E. (1999) *Phys. Chem. Chem. Phys.* **1,** 1431–1440.
19. Steuhl, H. M., Bornemann, C. & Klessinger, M. (1999) *Chem. Eur. J.* **5,** 2404–2412.
20. Hertwig, A., Hippler, H., Schmid, H. & Unterreiner, A.-N. (1999) *Phys. Chem. Chem. Phys.* **1,** 5129–5132.
21. Paulick, W., Jung, C., Kempka, U., Suhnel, J. & Gustav, K. (1981) *Theochem* **2,** 235–240.
22. Møller, K. B. & Zewail, A. H. (1998) *Chem. Phys. Lett.* **295,** 1–10.
23. Diau, E. W.-G., Feyter, S. D. & Zewail, A. H. (1999) *J. Chem. Phys.* **110,** 9785–9788.
24. Yan, M., Rothberg, L. & Callender, R. (2001) *J. Phys. Chem. B* **105,** 856–859.
25. Lawless, M. K., Wickham, S. D. & Mathies, R. A. (1995) *Acc. Chem. Res.* **28,** 493–502.
26. Lochbrunner, S., Fuss, W., Schmid, W. E. & Kompa, K. L. (1998) *J. Phys. Chem. A* **102,** 9334–9344.
27. Anderson, N. A., Pullen, S. H., Walker, L. A., Shiang, J. J. & Sension, R. J. (1998) *J. Phys. Chem. A* **102,** 10588–10598.
28. Fuss, W., Schmid, W. E. & Trushin, S. A. (2000) *J. Chem. Phys.* **112,** 8347–8362.
29. Clary, D. C. (2001) *J. Chem. Phys.*, in press.
30. Minnard, N. G. & Havinga, E. (1973) *Recl. Trav. Chim.* **92,** 1315–1320.
31. Garavelli, M., Bernardi, F., Olivucci, M., Vreven, T., Klein, S., Celani, P. & Robb, M. A. (1998) *Faraday Discuss.* **110,** 51–70.
32. Mizutani, Y., Uesugi, Y. & Kitagawa, T. (1999) *J. Chem. Phys.* **111,** 8950–8962.
33. Helliwell, J. R. & Rentzepis, P. M. (1997) *Time-Resolved Diffraction* (Oxford Univ. Press, New York).
34. Rousse, A., Rischel, C., Fourmaux, S., Uschmann, I., Sebban, S., Grillon, G., Balcou, P., Forster, E., Geindre, J. P., Audebert, P., *et al.* (2001) *Nature (London)* **410,** 65–68.
35. Techert, S., Schotte, F. & Wulff, M. (2001) *Phys. Rev. Lett.* **86,** 2030–2033.
36. Lauro, C. D. & Neto, N. (1969) *J. Mol. Struct.* **3,** 219–226.
37. Panchenko, Y. N., Krasnoshchiokov, S. V., George, P. & Bock, C. W. (1992) *Struct. Chem.* **3,** 15–26.
38. Frisch, M. J., Trucks, G. W., Schlegel, H. B., Scuseria, G. E., Robb, M. A., Cheeseman, J. R., Zakrzewski, V. G., Petersson, G. A., Montgomery, S. A., Jr., Stratman, R. E., *et al.* (1998) GAUSSIAN 98 (Gaussian, Pittsburgh, PA).